Unequal Compressive Imaging

Betelhem Mekisso, Ali Talari and Nazanin Rahnavard
Oklahoma State University, Stillwater, OK 74078
Emails: {betelhe, ali.talari, nazanin.rahnavard}@okstate.edu

***Abstract*—Recently, novel *compressive sensing* (CS) techniques have been employed to concurrently perform compression and image sampling. Since an image has *sparse* representation in some proper transform basis, such as *discrete cosine transform* (DCT) and *wavelet transform*, we can reconstruct it from its undersampled random projections called *measurements* employing CS techniques.**

We consider the fact that the area in an image that contains the main subject, such as the face in a portrait, is more important to viewers. We employ an existing algorithm from image processing area to find the area of the images that corresponds the main subject, and propose to directly apply unequal compressive sampling on coefficients of this area. With this setup, the main subject is reconstructed with a higher accuracy, while the less important areas are slightly degraded. Unequal compressive imaging is mainly inspired by a previous work by Rahnavard et al. on *unequal error protection rateless codes*.

I. Introduction

Conventional image compression algorithms as used in digital cameras, directly take a snapshot of the whole image *coefficients* (pixels). Next, by projecting the image coefficients into another basis, e.g., *discrete cosine transform* (DCT) in JPEG, a sparse representation of the image with many close to zero entries is obtained [1]. These small coefficients may be discarded without causing perceptual loss of image quality and result in a compressed image.

Consider an $\sqrt{N} \times \sqrt{N}$ image with N coefficients $\underline{x} \in \mathbb{R}^N$ (i.e. $\underline{x} = [x_1, x_2, x_3 \cdots ...x_N]$). Further, let $\underline{s} \in \mathbb{R}^N$ (i.e. $\underline{s} = [s_1, s_2, s_3 ... s_N]$) be the sparse representation of $\underline{x}$ in DCT or *wavelet* basis $\Psi \in \mathbb{R}^{N \times N}$, i.e., $\underline{x} = \Psi \underline{s}$. Such a sparse representation is actually the compressed transform of $\underline{x}$ with only $K \ll N$ *significant* coefficients and many *near-zero* coefficients. *Compressive sensing* (CS) techniques exploit the described compressibility of the images and show that we may recover the image $\underline{x}$ from only $M \ll N$ *random projections* (measurements), where $M \geq O(K \log N)$ [2].

The M random projections are generated by $\underline{y} = \Phi \underline{x} = \Phi \Psi \underline{s}$, where $\Phi \in \mathbb{R}^{M \times N}$ is called measurement (projection) matrix. Examples of measurement matrices are matrices with entries randomly selected from $\{+1, 0, -1\}$ or $\mathcal{N}(0, 1)$ [2]. Image reconstruction can be done by finding the estimate $\hat{\underline{s}}$ from the system of linear equations $\underline{y} = \Phi \Psi \underline{s}$. This is an underdetermined system with infinitely many solutions. It has been shown that $\hat{\underline{s}}$, the estimate of $\underline{s}$, is the solution to the following ℓ_1 optimization problem [3–6]:

$$\hat{\underline{s}} = \text{argmin} \|\underline{s}\|_1, \text{ s.t. } \underline{y} = \Phi \Psi \underline{s}, \tag{1}$$

where $\|\underline{s}\|_1 = \sum_{i=1}^{N} |s_i|$. Finally, the reconstructed image is obtained by $\hat{\underline{x}} = \Psi \hat{\underline{s}}$.

In this paper, we mainly focus on the construction of new measurement matrices for compressive imaging applications. We assume that an image $\underline{x}$ is directly sampled in the spatial domain. Clearly, images contain at least one *main subject* that communicates the information of the image and attracts viewers attention. For instance, the quality of the face part of images in a digital photograph library is more important than the rest of the image and attracts viewers attention. Therefore, we adopt a novel *main subject detection* algorithm [7] from image processing area to identify the main subject and this part of the image is assumed to be more important than the rest of the image. Next, we propose to design a Φ matrix such that the area of the image embracing the main subject of the image is more protected. This considerably improves the perceptual quality of the main subject in the image which is more important than the rest of the image. To the best of our knowledge, this is the first work that modifies the *encoding phase* (measurement generation) of CS to provide unequal error protection property (UEP) for the CS technology on images.

This paper is organized as follows. Section II, briefly reviews the related work. In Section III, we describe our UEP algorithm for CS on images and evaluate its performance. Finally, Section IV concludes the paper.

II. Related Work

Dense measurement matrices have been used in most of the early CS algorithms [8], [2]. In most algorithms, such dense measurement matrices are constructed in such a way that the entries in each row are selected independently from some distribution such as Bernoulli or Gaussian. Such dense measurement matrices however have major disadvantages on the required encoding and decoding times. The scrambled Fourier ensemble (SFE) [9], [10] have been proposed for compressive imaging applications and were shown to provide fast CS computation. However, these matrices are also dense and hence they still require huge buffer sizes.

Low density parity check (LDPC) like measurement matrices have, recently, been proposed as they provide fast encoding and decoding times as a result of fast matrix multiplications [11], [12], [13]. In contribution [12], a binary sparse measurement matrix is proposed which has a fixed number of ones in each column. Such sparse measurement matrices were also shown to perform as good as dense Gaussian and Fourier matrices when used with LP decoding. Furthermore, the LP decoding is shown to be faster when sparse measurement matrices are used.

All these proposed matrices recover each coefficients of a given signal with equal probability. We, however, propose a sparse measurement matrix which provides CS with a functionality of recovering different signal coefficients with different probabilities.

III. UEP for Main Subject in Images

In this section, we propose a compressive imaging algorithm, which samples images non-uniformly, so as to provide more recovery quality for the region of interest (ROI) of images.

A. Non-Uniform Importance of Areas in Images

It is known that compressive sampling is performed as $\underline{y} = \Phi\underline{x}$. Where $\underline{y}$ is the measurement, Φ is the measurement matrix and $\underline{x}$ is the object of interest (image). In practice most images have a main subject, usually located in the center of the image, which is of interest to the viewer. Therefore, we may sacrifice the quality of less important areas of the image, e.g., blurry background that convey less important information to improve the quality of the area containing the main subject. For this scenario, we propose UEP measurement matrix (Φ) for the non-sparse representation of image coefficients $\underline{x}$, to provide more protection on the more important areas of images. As we later see, the degradation in the less important areas when a UEP-Φ is employed is usually not perceived by viewers, while the improvement made in the important image part is significantly noticeable.

To implement our proposed idea, we adopt a novel main subject detection algorithm proposed in [7]. This algorithm outputs the area of the image that contains the main subject. Therefore, the coefficients of $\underline{x}$ that represent the part of the image identified as the main subject are considered as MICs and the rest of coefficients are considered as LICs. It is important to note that the MIC coefficients might not be found in continuous locations and could be spread throughout the signal $\underline{x}$. We have exemplified this in Lena's image in Figure 1, where the image has been divided into five blocks. The shaded area in vector $\underline{x}$ correspond to Lena's face (MICs). Further, we perform the main subject detection algorithm of [7] on images from Microsoft Research database [1] and shown the results in Figure 2.

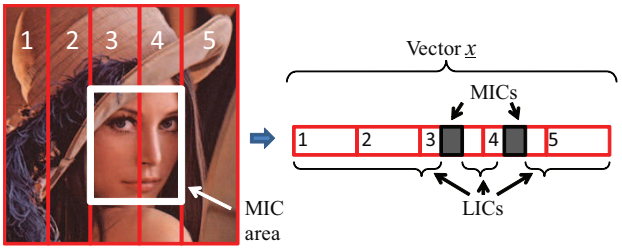

Fig. 1. Main subject detection and distribution of its corresponding coefficients in $\underline{x}$.

[1] http://research.microsoft.com/en-us/projects/objectclassrecognition/

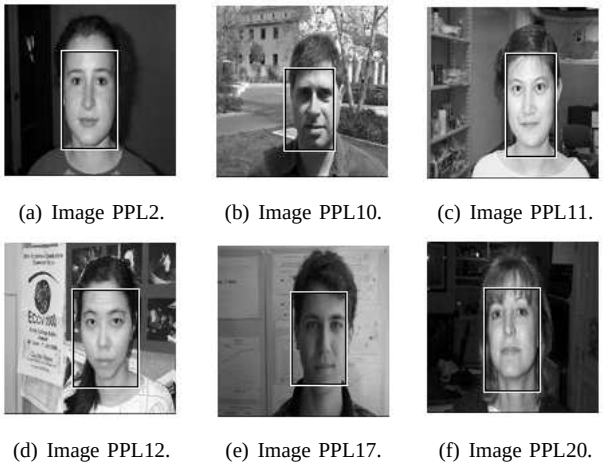

(a) Image PPL2. (b) Image PPL10. (c) Image PPL11.

(d) Image PPL12. (e) Image PPL17. (f) Image PPL20.

Fig. 2. Main subject detection algorithm output on sample images.

B. Non-Uniform Protection of Important Areas

Sparse Gaussian ϕ matrix is implemented in our algorithm as sparse ϕ matrices perform almost as good as dense ones and further provide less computational complexity for CS [12]. The performance comparison between dense and sparse ϕ matrices is shown in Figure 3. This figure shows the VIF of Lena images reconstructed with dense Gaussian, sparse Gaussian and sparse binary ϕ matrices when different number of measurements (M) are taken. The number of measurements are chosen to represent small($M = 2000$, $M = 4000$), medium ($M = 6000$) and large ($M = 8000$) number of measurements. The entries of the sparse and dense Gaussian matrices are taken from independent and identically distributed (i.i.d.) Gaussian distribution while the entries of the sparse binary ϕ matrix are zeros and ones. The sparse ϕ matrices are constructed with 8 non-zero entries in each row which are placed uniformly at random.

As it could be seen from Figure 3, there is only small performance loss when using sparse measurement matrices. Sparse Gaussian ϕ matrix is implemented for our algorithm because such matrices are incoherent with any basis of sparsity ψ with high probability (universality property) [12]. Furthermore, employing a sparse Φ allows us to design Φ matrices to provide UEP. Moreover, as we later see the slight performance loss of sparse Φ matrices, as compared to the dense ones, only occurs with *equal error protection* (EEP) setup and UEP-Φ surpasses the reconstruction performance of a dense Φ.

Let $L \ll N$ be the number of non-zero entries in each row of sparse Φ. In an EEP setup with a sparse ϕ, these L non-zero elements are placed uniformly at random across the columns of each row and independent of other rows. Therefore, $\phi_{i,j}$ the element on the i^{th} row and j^{th} column of Φ is an entry from iid Gaussian distribution or a zero with probabilities $\frac{L}{N}$ and $\frac{N-L}{N}$, respectively. This would clearly provide a uniform capturing of $\underline{x}$ coefficients by M measurements ($\underline{y}$).

However, as we discussed in the previous section, we have the knowledge of where the important coefficients are located

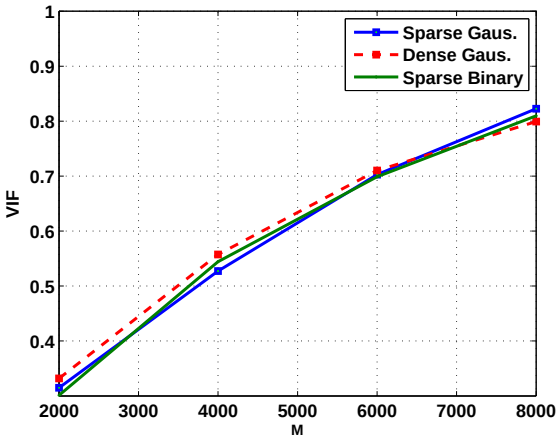

Fig. 3. comparison of VIF for dense and sparse Gaussian matrices.

in $\underline{x}$. Consequently, employing the idea of UEP erasure coding from [14, 15], we propose to concentrate the L non-zero elements of Φ at its columns which sample the important coefficients of $\underline{x}$. With this setup, more important coefficients are incorporated in the generation of more measurements. Therefore, in CS reconstruction they will be recovered with a higher accuracy.

Therefore, for the sake of simplicity and without loss of generality we assume that N coefficients of $\underline{x}$ are grouped into two levels of importance[2]. Let α fraction of N coefficients be *more important coefficients* (MICs) and $1-\alpha$ fraction be *less important coefficients* (LICs). Clearly, $n_1 = \alpha N$ columns of Φ capture MICs and the rest $n_2 = (1-\alpha)N$ capture LICs.

Let P_1 be the probability that an element in the columns of a particular row of ϕ which captures an MIC will be a non-zero. And let P_2 be the probability that an element in the columns of a particular row of ϕ which captures an LIC will be a non-zero. Further, let us define $P_1 = \frac{k_M}{N}$ and $P_2 = \frac{k_L}{N}$, where k_M and $k_L = \frac{1-\alpha k_M}{1-\alpha}$ are the *protection levels*. Clearly, UEP- and EEP-Φ matrices are built by setting $k_M > k_L$ and $k_M = k_L = 1$, respectively.

For all simulations presented in this paper, we assume a regular *basis pursuit* (BP) reconstruction algorithm [6] (which is designed employing linear programming techniques) is employed to solve the CS reconstruction problem:

$$\hat{\underline{x}} = \text{argmin}\|\underline{x}\|_1, \text{ s.t. } \underline{y} = \Phi\underline{x}. \tag{2}$$

Among the image quality assessment measures, we employ the *visual information fidelity* (VIF) [16] as it is able to measure image quality that relates with visual perception. Note that VIF of a reconstructed image varies between 0 and 1, where a value closer to 1 shows a closer reconstructed image to the original image.

[2]We may also consider more than two levels of importance. However, this only increases the complexity of the problem while not improving the contribution.

In the next subsections, we obtain the optimal values for the parameters of our proposed algorithm, implement the algorithm on the sample images and evaluate its performance.

C. Optimal Parameter values

Several experiments were carried out using the sample images, shown in Figure 2, in order to find the optimal value for the different parameters involving the proposed UEP ϕ. Figure 4 shows the reconstruction quality of Lena image at different L and k_M values when $\alpha \approx 0.15$ at $M = 6000$ and $M = 8192$.

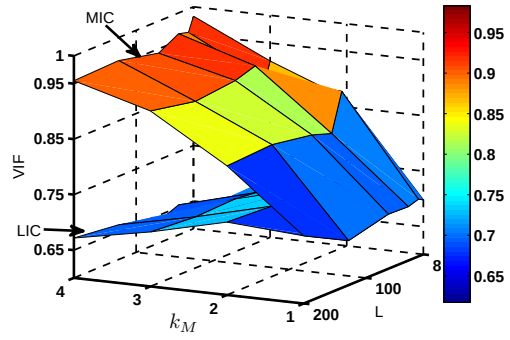

(a) M=6000

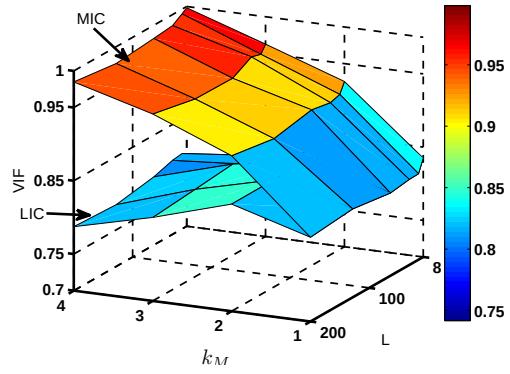

(b) M=8192

Fig. 4. VIF of reconstructed Lena image at M=6000 and M=8192 for different k_M and L values.

As it could be seen from Figure 4, different values of L result in similar reconstruction quality for all k_M values. However, the CPU time is significantly higher when a large value of L is used. Figure 4 also shows that the quality of the MICs increases while that of the LICs decreases when increasing the value of k_M. However, the performance of neither the MICs nor the LICs show significant change with various L values. As it could be seen in the figure, this relationship is observed at both $M = 6000$ and $M = 8192$. The only difference observed when varying the number of measurements M is the graph as a whole moves up for larger M values and it moves down for smaller values. Similar results were obtained for all the images experimented with, for different number of measurements M and also when the

wavelet basis is used as the basis of sparsity, ψ. A row weight of 16, $L = 16$, is thus chosen to be the optimal row weight in order to achieve fast encoding/decoding process.

Another parameter that is important for UEP on CS is the size of the image that is selected to be the region of interest (ROI) as compared to the size of the whole image, which is represented by α. Figure 5 below shows the reconstruction quality of Lena image at different α and k_M values when $M = 8192$, $L = 16$ and implementing the DCT as the basis of sparsity, ψ.

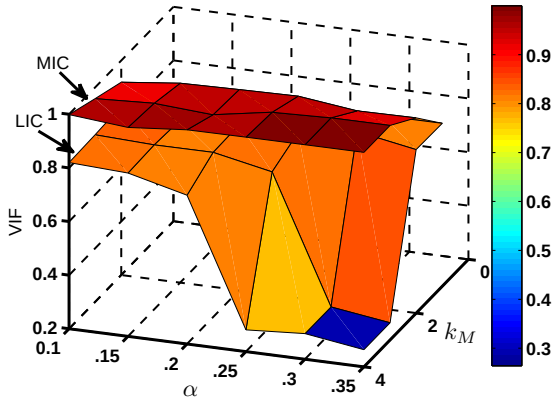

Fig. 5. VIF of reconstructed Lena image at M=8192 and L=16 for different α and k_M values.

As it could be seen from Figure 5, a small size of ROI could be reconstructed in such a way that the ROI is recovered with a quality better than the background whereas the background is also reconstructed with an acceptable quality. Where as, the quality of the background significantly drops to an unacceptable level when large ROIs are used. This is because, as the size of the ROI is large, most non-zeros would be allocated for columns of ϕ sampling the ROI while the rest columns have insufficient non-zero entries to successfully sample the background. Note that the MICs represent the ROI while the LICs represent the background.

Another interesting relationship could be observed between k_M values and MIC sizes from Figure 5. It could be seen that it is possible to reconstruct large ROIs with a quality better the background while the background is also reconstructed with an acceptable quality by using small k_M values. In Figure 5, for example, the quality of the LICs is very low for $\alpha = 0.25$ when $k_M = 4$. However, it could be seen that the LICs are reconstructed with a significantly better quality when the k_M value is decreased to $k_M = 3$. The trade off is that when a smaller k_M value is used, the difference between the quality of MICs and LICs decreases with $k_M = 1$ being EEP where the ROI and the background have similar qualities.

As it could be seen in Figure 5, the maximum MIC size that results in acceptable recovery of LICs for a k_M value of 4 is obtained when $\alpha \approx 0.2$ (i.e. when the ROI covers 20% of the whole image coefficients). Similar result was obtained for a k_M value of 5. The largest of the ROIs for the sample images shown in Figure 2 approximately covers 20% of the whole image ($\alpha \approx 0.2$). The size of the ROIs (main subject) was purposely made to be of this small size by adopting a slight modification in the MSD algorithm [7]. Moreover, a k_M value of $k_M = 5$ and $k_M = 4$ are used according to the size of the ROIs of the sample images.

D. Relationship between parameters and image quality

In this subsection, we discuss how the reconstructed image quality varies with the number of measurements, M, and the protection level k_M. It has been mentioned earlier that results similar to those shown in Figures 4 and 5 are obtained for different number of measurements, M. From the theory of CS, it is known that the reconstruction error decreases when the number of measurements, M, is increased. As a result, it is clear that even though similar pattern as that of Figures 4 and 5 is obtained with different M values, the actual VIF values increase when M is large and decrease when M is small. This is clearly seen in Figure 4.

Figure 6 shows the reconstruction quality of the Lena image at different number of measurements, M. The results are presented for EEP ($k_M = 1$) and UEP ($k_M = 4$). The row weight is set to a value of 16, $L = 16$, in both cases. A very important observation that could be made from Figure 6 is the successfulness of UEP. More precisely, it could be seen that the quality of the ROI (VIF of MICs) is significantly better than the background (VIF of LICs). Moreover, the background is recovered with a quality that is as good as the EEP.

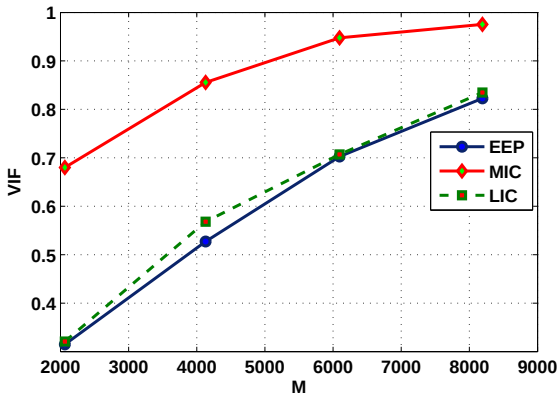

Fig. 6. Reconstruction quality of Lena image for k_M = 4, L = 16 and $\alpha \approx 0.15$ at different M values.

Figure 7 further emphasizes the relationship between the VIF of ROIs (MICs) and background (LICs) which could also be observed in Figure 5. The result shown in Figure 7 is for the Lena image when $M = 8192$, $\alpha \approx 0.15$ and $L = 16$. It could be seen from this figure that the quality of the ROI increases when high k_M values are used where as the background is recovered with a quality as good as that of EEP($k_M = 1$). It should however be noted that the size of the ROI must be appropriate according to the the discussion in Section III-C for this relationship to hold.

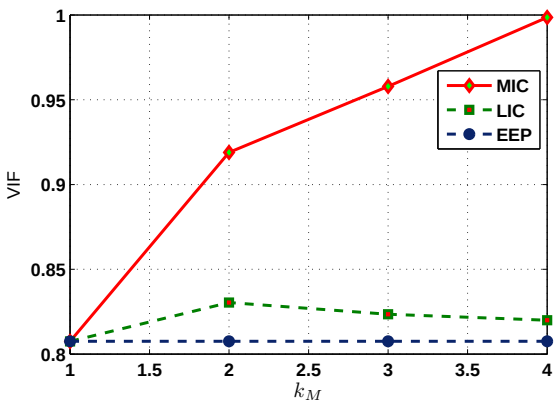

Fig. 7. Reconstruction quality of Lena image for M = 8192 and $\alpha \approx 0.15$ at different k_M values.

E. Representative Results

We perform our simulations with optimal parameters on images shown in Figure 2. We first resize all images to a size of 128×128, resulting a total number of 16,384 coefficients ($N = 16,384$). Then, the optimal parameter values discussed in subsection III-C are used to obtain the simulation results presented in this subsection. The number of measurement used for results presented in Table I is $M = 6000$. A row weight value of $L = 16$ is used for all simulations while a k_M value of k_M=5 is used for all the images except for sample images PPL12 and PPL20. A k_M value of k_M=4 is used for PPL12 and PPL20 due to their large α values (please refer Table I for the α values of the images).

In Table I, we compare the VIF of MIC area, LIC area, and the whole image for UEP-Φ encoding versus encoding with sparse and dense EEP-Φs. The VIF for EEP is computed for the whole image. On the other hand, the VIF for UEP is computed for the image as a whole and also for the MICs and LICs separately. The VIF computed for the part of an image identified as the ROI, which is shown under a rectangle in Figure 2, is shown as the VIF for the MIC. In a similar way, the VIF computed for the whole image excluding the main subject is shown as the VIF for the LIC whereas the VIF of the whole image is shown as total VIF.

TABLE I
VIF OF CS RECONSTRUCTION PERFORMANCE EMPLOYING EEP-Φ AND UEP-Φ.

Images		PPL2	PPL10	PPL11	PPL12	PPL17	PPL20
α		0.18	0.13	0.17	0.21	0.17	0.19
EEP	Sparse Φ	0.83	0.67	0.75	0.69	0.81	0.8
	Dense Φ	0.85	0.64	0.78	0.71	0.82	0.77
UEP	MIC	1	0.98	0.99	0.96	1	0.97
	LIC	0.81	0.64	0.74	0.69	0.84	0.76
	Total	0.87	0.68	0.77	0.71	0.84	0.85

From Table I, we can see that when UEP-Φ is employed in the encoding phase a considerable improvement is obtained for the region of interest (ROI) at the expense of a small quality loss in the background. For instance, for the image PPL2, the VIF of MIC has increased from 0.85 (for dense EEP-Φ) to 1 (a perfect reconstruction), while the VIF of LIC has a small decrease from 0.81 to 0.85. Therefore, the deterioration in the background may not even be noticed even though the region of interest (ROI) has been reconstructed with a quality very close to the original. This could be clearly seen in Figure 8, where a sample image reconstructed with our proposed algorithm is presented along with reconstructions resulting from the sparse and dense EEP-Φ matrices at $M = 6000$ for visual comparison. Note that, since α is not equal for all the sample images, we can see various reconstruction improvements for different images in Table I. As MIC area becomes smaller, its corresponding reconstruction quality increases and the quality of LIC is more preserved.

(a) MSD on original image. (b) Reconstruction by EEP-Φ.

(c) Reconstruction by dense Φ. (d) Reconstruction by UEP-Φ.

Fig. 8. Reconstruction quality comparison of UEP-ϕ versus dense and sparse EEP-ϕs for sample image PPL2. Here, $n = 16384$ and $m = 6000$.

From Figure 8, we can see that the ROI has been recovered with higher quality than the rest of image, while the degradation in the background is not significant. Similar results were obtained for all the sample images as shown in Table I.

IV. CONCLUSION

In this paper, we proposed to incorporate the *unequal error protection* (UEP) ideas from error correction codes into *compressive sensing* (CS) algorithm for image reconstruction. We proposed a novel measurement matrix construction for CS encoding phase where *higher protection* can be assigned to more important coefficients. It is well-known that images usually have an area, known as *main subject*, which communicates most of the image information. Therefore, we employed a well-known main subject detection algorithm to identify

the main subject of imageries. Next, we proposed to capture this area with better quality by incorporating its coefficients into more number of measurements. We observed that this would significantly improve the reconstruction quality of the area containing the main subject, while resulting in slight degradation in the less important areas such as background. Therefore, we have been able to better protect the region of interest of images by employing our proposed structure of UEP-Φ.

ACKNOWLEDGMENT

This material is based upon work supported by the National Science Foundation under Grant No. ECCS-1056065 and Microsoft Research.

REFERENCES

[1] L. He and L. Carin, "Exploiting structure in wavelet-based bayesian compressive sensing," *IEEE Trans. Signal Process*, vol. 57, number=9, pages=3488-3497, year=2009, month = September,.

[2] D. Donoho, "Compressed sensing," *IEEE Trans. Inform. Th.*, vol. 52, p. 12891306, Apr 2006.

[3] D. Donoho, "Compressed sensing," *IEEE Trans. on Information Theory*, vol. 52, no. 4, pp. 1289–1306, 2006.

[4] E. Candes, J. Romberg, and T. Tao, "Robust uncertainty principles: exact signal reconstruction from highly incomplete frequency information," *IEEE Trans. on Information Theory*, vol. 52, pp. 489–509, Feb. 2006.

[5] E. Candes and T. Tao, "Near-optimal signal recovery from random projections: Universal encoding strategies?," *IEEE Trans. on information theory*, vol. 52, no. 12, pp. 5406–5425, 2006.

[6] S. S. Chen, D. L. Donoho, Michael, and M. A. Saunders, "Atomic decomposition by basis pursuit," *SIAM Journal on Scientific Computing*, vol. 20, pp. 33–61, 1998.

[7] C. Vu and D. Chandler, "Main subject detection via adaptive feature selection," *IEEE Intl. Conf. on Image Processing*, pp. 3101 – 3104, November 2009.

[8] J. R. E. Cand'es and T. Tao, "Stable signal recovery from incomplete and inaccurate measurements," *Communications on Pure and Applied Mathematics*, vol. 59, pp. 1208–1223, Aug 2006.

[9] E. Cand'es and J. Romberg, "Robust signal recovery from incomplete observations," *Proceedings of International Conference on Image Processing*, vol. 59, pp. 1208–1223, Aug 2006.

[10] E. Cand'es and J. Romberg, "Practical signal recovery from random projections," *In Proceedings of SPIE Computational Imaging*, vol. 5674, no. 8, pp. 75–86, 2005.

[11] D. B. S. Sarvotham and R. Baraniuk, "Sudocodes-fast measurement and reconstruction of sparse signals," *In Proceedings of IEEE International Symposium on Information Theory*, pp. 2804 – 2808, Dec. 2006.

[12] R. Berinde and P. Indyk, "Sparse recovery using sparse random matrices," *MIT, Cambridge, MA, Tech. Rep. MIT-CSAIL-TR-2008-001*, 2008.

[13] S. S. D. Baron and R. G. Baraniuk, "Bayesian compressive sensing via belief propagation," *IEEE Trans. signal Process.*, vol. 58, pp. 269–280, 2010 Jan.

[14] N. Rahnavard, B. Vellambi, and F. Fekri, "Rateless codes with unequal error protection property," *IEEE Transactions on Information Theory*, vol. 53, pp. 1521–1532, April 2007.

[15] N. Rahnavard and F. Fekri, "Generalization of rateless codes for unequal error protection and recovery time: Asymptotic analysis," *IEEE International Symposium on Information Theory, 2006*, pp. 523–527, July 2006.

[16] H. Sheikh and A. Bovik, "Image information and visual quality," *IEEE Transactions on Image Processing*, vol. 15, no. 2, pp. 430 –444, 2006.